01 Oct 2005

QCA-Based Majority Gate Design under Radius of Effect-Induced Faults

Zachary D. Patitz

Nohpill Park

Minsu Choi
Missouri University of Science and Technology, choim@mst.edu

Fred J. Meyer

Recommended Citation

Z. D. Patitz et al., "QCA-Based Majority Gate Design under Radius of Effect-Induced Faults," *Proceedings of the 20th IEEE International Symposium on Defect and Fault Tolerance in VLSI Systems (2005, Monterey, CA)*, pp. 217-225, IEEE Computer Society, Oct 2005.
The definitive version is available at https://doi.org/10.1109/DFTVS.2005.55

QCA-Based Majority Gate Design under Radius of Effect-Induced Faults

Zachary D. Patitz[1], Nohpill Park[1], Minsu Choi[2] and Fred J. Meyer[3]
[1] Dept of CS, Oklahoma State University
Stillwater, OK 74078, {patitzz, npark}@cs.okstate.edu
[2] Dept of ECE, University of Missouri-Rolla
Rolla, MO 65409, choim@umr.edu
[3] Dept of ECE, Wichita State University
Wichita, KS 67260, fred.meyer@wichita.edu

Abstract

This paper presents reliable QCA cell structures for designing single clock-controlled majority gates with a tolerance to radius of effect-induced faults, for use as a basic building component for carry look-ahead adder. Realizable quantum computing is still well in the future due to the complexity of the quantum mechanics that govern them. In this regard, QCA-based system design is a challenging task since each cell's state must interact with all the cells that are in its energy-effective range in its clocking zone, referred to as its radius of effect. This paper proposes a design approach for majority gates to overcome the constraints imposed by the radius of effect of each cell with respect to clock controls. Radius of effect induces faults that lead to constraints on the clocking scheme of majority gates. We will show majority gate structures that will operate with multiple radius of effect-induced faults under a single clock control. The proposed design approach to a single clock controlled majority gate will ultimately facilitate more efficient and flexible clocking schemes for complex QCA designs.

1: Introduction

QCA (Quantum-Dot Cellular Automata) is one of the six promising technologies for nano-scale computing listed in the Industry Technology Roadmap for Semiconductors (ITRS) 2004 [1]. In the QCA paradigm, a regular array of cells, each interacting with its neighboring cells, is employed in a locally interconnected architecture [2–8]. The coupling between the cells is given by their electrostatic interactions. Such arrays are in principle capable of encoding digital information. The fundamental unit of QCA is the QCA cell created with four quantum dots positioned at the vertices of a square. The cell is loaded with two extra electrons which tend to occupy the diagonals due to electrostatic repulsion. Binary information is encoded in the two possible polarizations (i.e., +1 or -1). The cell will switch from one polarization to the other when the electrons quantum-mechanically tunnel from one set of dot positions to the other [9]. Implementing QCA cells with single molecules is a new area with considerable promise. It is anticipated that molecular QCA architectures could operate at densities 10^{12} devices/cm^2 and 100 GHz domain [10, 11].

One of the major hurdles that needs to be overcome in quantum computing is defect- and fault-tolerance. Quantum-dot cellular automata (QCA) are no different in this respect. QCA are composed of a number of cells each of which contains four dots where electrons may lie. The small structures are subject to manufacturing defects as well as other faults. A QCA cell may interact with too many of its neighboring cells and cause erroneous operation of the most basic functions.

Proceedings of the 2005 20th IEEE International Symposium on Defect and Fault Tolerance in VLSI Systems (DFT'05)
0-7695-2464-8/05 $20.00 © 2005 IEEE

Also, use of fine-grained complex clocking zones may result in more reliable operations, but it induces excessive complexity of underlying clocking wire structure and additional time delay. In order to address these issues, this paper proposes a design strategy involving design elements robust to radius of effect-induced faults, here, the majority gate. The proposed fault-tolerant majority gate can be placed in a single clocking zone; therefore, it will also be useful for designing QCA circuits with less complex clocking structures.

In section 2, we will briefly discuss QCA cells and basic structures that are used to create complex arrays for computation, the clocking scheme that is used to control large arrays of cells and the faults that can occur due to an increase or a decrease within the radius of effect of each cell. Section 3 introduces structures that can tolerate various radius of effect-induced faults while under only a single clock control to perform a majority gate operation. Simulation results for the structures will be shown as well. The conclusion will reflect the impact that these modified majority gates are predicted to have on the future of quantum-dot cellular automata and their introduction into the world in the form of viable quantum computers.

2: Preliminaries and Review

A QCA-based implementation of a single carry-look-ahead full-adder is a target design in which the proposed single clock-controlled majority-gate is employed as a basic component, which will ultimately facilitate a multi-staged pipelined processor design. In order to construct the proposed single carry-look-ahead full-adder under a single clock control (one set of four clock phases), the proposed majority gates are to be integrated along with proper clocking, wire crossings and inverter wires. In order to create a functional full adder, three inputs are needed: a, b, and C_{in}. A design of the single carry-look-ahead full-adder is shown in Figure 1 as created using QCADesigner, a design, layout and simulation tool for QCA [12, 13]. As derived in [19] the formulae used in the creation of the adder are as follows:

$$C_{out} = m(a, b, C_{in}) \tag{1}$$

$$Sum = m(m(\overline{a}, b, C_{in}), m(a, \overline{b}, C_{in}), m(a, b, \overline{C}_{in})) \tag{2}$$

Where m defines the three-input majority function as previously discussed. The adder uses three, four-phase clocks; each phase consumes a zone with a width of three cells. The three cells of each zone are adjacent and each zone runs vertically down the array, as would occur with the previously discussed clocking scheme.

The clocking scheme used for this adder is the same as was discussed in the previous section. Figure 1 differentiates between clocking zones by shading. Each clocking zone in this example has a three cell width, under which run wires that produce the corresponding phase of that zone. The speed of the wire transitions, and, therefore, the clock, is directly related to the longest path of cells in any one zone. In the case of our adder, that longest path is 32 cells in the 5^{th}, 6^{th} and 7^{th} zones. These are the zones that contain the vertical inverter wires.

3: Radius of Effect-Induced Faults

The radius of effect of each cell can and will affect the operation of certain structures in a QCA array. In this section we will analyze a simple majority gate using the QCADesigner [13] under a single clock control and using different areas within the radius of effect. The radius of effect-induced faults will become apparent through a few simple simulations.

The radius of effect of a cell is the radius at which it will interact with other cells. In the simulator, specifications of the radius of effect is from the center of one cell to the center of another. So two in-line cells will interact if

$$d = d_N = w + s \tag{3}$$

Proceedings of the 2005 20th IEEE International Symposium on Defect and Fault Tolerance in VLSI Systems (DFT'05)
0-7695-2464-8/05 $20.00 © 2005 IEEE

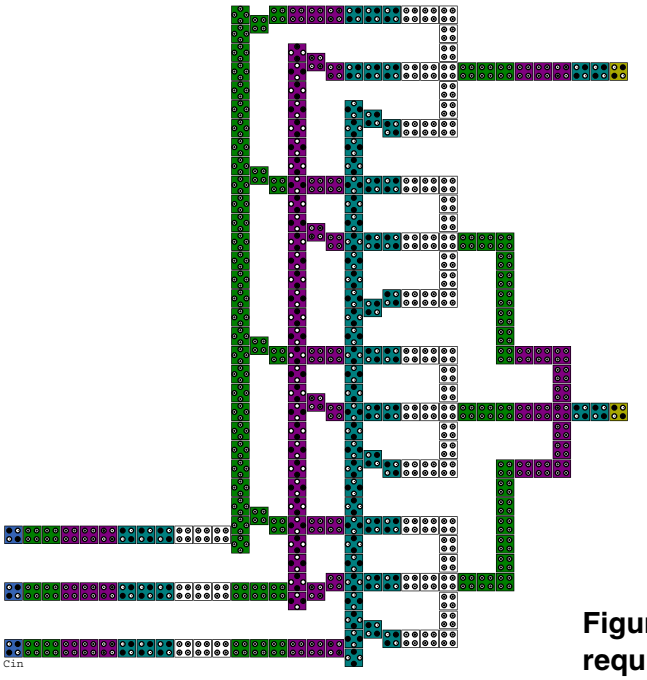

Figure 1. A single carry-look-ahead full-adder.

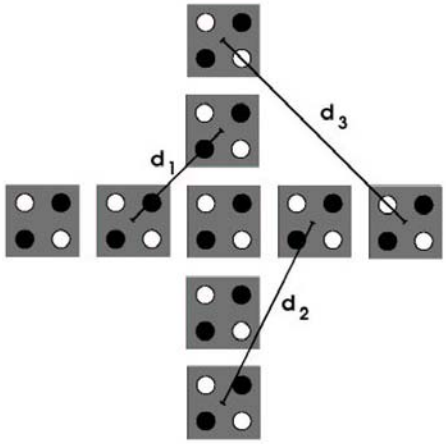

Figure 2. Area of effect distances which require consideration.

where d is the radius of effect, w is the width (and height) of the (square) cell, and s is the distance of separation of the cell. Now we will specify the distances that will be used in testing. We will test the majority gate at different areas within the radius of effect. We will assume that the cells are evenly spaced and of uniform width and height. The cells that are being used in these simulations are 20 nm by 20 nm with 5 nm dots. The cells are spaced 5 nm apart.

Equation 3 is the distance for nearest neighbor which we will denote as d_N. The radius of effect for next to nearest neighbor will simply be

$$d_{NN} = 2(d_N) = 2w + 2s \tag{4}$$

Using the Pythagorean theorem, we can find some of the other important distances that need to be considered in testing the area within the radius of effect. For the diagonal cell distances (see Figure 2), which we will call first diagonal, second diagonal and third diagonal, respectively, we have the three equations

$$d_1 = \sqrt{2((s+w)^2)} \tag{5}$$

$$d_2 = \sqrt{(s+w)^2 + (2s+2w)^2} \tag{6}$$

$$d_3 = \sqrt{2((2s+2w)^2)} \tag{7}$$

We limit the area of effect distances to d_3 due to the rapid decay of kink energy between cells as their distance of separation increases. As stated in [12], it decreases inversely with the fifth power of the distance of cell separation.

Now that we have the distances of note defined, we can analyze their impact on a majority gate. We will use the coherence-vector simulation to test. The i^{th} cell simulated in the coherence vector simulation is a two-state cell and is defined by the Hamiltonian [12]

$$H_i = \sum_{j \epsilon S} \begin{pmatrix} -\frac{1}{2} P_j E^k_{i,j} & -\gamma_i \\ -\gamma_i & +\frac{1}{2} P_j E^k_{i,j} \end{pmatrix}. \tag{8}$$

Proceedings of the 2005 20th IEEE International Symposium on Defect and Fault Tolerance in VLSI Systems (DFT'05)
0-7695-2464-8/05 $20.00 © 2005 IEEE

Table 1. Radius of Effect Testing Results

Radius of Effect	5 Cell Gate	9 Cell Gate	13 Cell Gate
$d_N \leq d < d_1$	Fault-free	Fault-free	Fault-free
$d_1 \leq d < d_{NN}$	Fault-free	Fault-free	$\overline{A}$
$d_{NN} \leq d < d_2$	Fault-free	B	$M(\overline{A}, B, \overline{C})$
$d_2 \leq d < d_3$	Fault-free	B	B
$d = d_3$	Fault-free	B	B

The energy needed to tunnel between polarization states is γ. The j^{th} cells indicate those cells that are in the effective radius of the i^{th} cell; S is the effective neighborhood of cell i. $E^k_{i,j}$ is the kink energy between the i^{th} and j^{th} cells and P_j is the polarity of the j^{th} cell. The kink energy (the cost of two cells having opposite polarities) $E^k_{i,j}$ can be found by calculating from the electrostatic interaction of all the charges. For each dot in i we compute its electrostatic interaction with each dot in j by using the equation [12]

$$E^k_{i,j} = \frac{1}{4\pi\epsilon_0\epsilon_r}\frac{q_i q_j}{|r_i r_j|} \tag{9}$$

where ϵ_0 is the relative permittivity of free space and ϵ_r is the relative permittivity of the system [12]. For clarity we will expand the equation for kink energy between two cells. The expanded form is

$$E^k_{i,j} = \frac{1}{4\pi\epsilon_0\epsilon_r}\sum_{i=0}^{3}\sum_{j=0}^{3}\frac{q^1_i q^2_j - q^1_i q^1_j}{|r_i - r_j|} \tag{10}$$

for $q^1_i = -0.8e-19$ for even i and $= 0.8e-19$ for odd i; $q^2_i = 0.8e-19$ for even i and $= -0.8e-19$ for odd i. The constant $0.8e-19$ is one half of one electron volt (eV), a half charge. The term $|r_i - r_j|$ is simply the distance between dot i in cell 1 and dot j in cell 2.

The results of the testing can be seen in Table 1, where the five-cell majority gate is the basic five-cell gate, and the nine-cell configuration is like that in Figure 2, with inputs from top, left and bottom, and output to the right. The thirteen-cell majority gate is expanded in the same way. The table gives the resulting outputs from the given configurations. A "Fault-free" table entry indicates that the gate functioned properly and the output was $M(A, B, C)$. Erroneous outputs are indicated by the differing output calculated by the simulator. The only usable erroneous output is for the 13-cell design with $d_{NN} \leq d \leq d_2$.

Looking at the table we can see how the radius of effect-induced fault disrupts the larger majority gates. The distance that works in all three instances is the nearest neighbor (d_N). This is obvious since the cells will only be interacting with at most four cells (the middle cell of the majority gate is within d_N of one cell above, below, to its left and to its right). For all distances the 5-cell configuration works, since this is the 'classic' setup for a majority gate with the results as expected.

The 9-cell gate obviously has more potential for more complex interaction and thus more potential for erroneous interaction. As can be seen in Table 1, there are only two distances that work. When setting the distance to d_{NN} or d_2, the output for the gate is equal to the left input value. The results are then erroneous. There is a rather serious problem here which we will now address.

Simple wire crossings require that there be at least next to nearest neighbor interaction. Without a radius of effect greater or equal to d_{NN} a wire crossing simply is not possible.

Now we can look back at Figure 1 to further illustrate the radius of effect problem. In the adder we see that the majority gates needed for the computation are constructed as shown in Figure 3, which we refer to as a *left-to-right majority gate*. The results of a coherence-vector simulation of this configuration with a radius of effect of d_{NN} can be seen in Figure 8 as erroneous. The resulting output is as if the top input, input A were flipped, i.e., $M(\overline{A}, B, C)$. This type of majority gate is used four times in the single carry-look-ahead adder. The adder works, however, due to its clocking

Proceedings of the 2005 20th IEEE International Symposium on Defect and Fault Tolerance in VLSI Systems (DFT'05)
0-7695-2464-8/05 $20.00 © 2005 IEEE

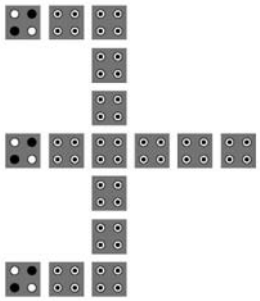

Figure 3. Left to right majority gate as used in an adder constructed of 20nm x 2 0nm cells with 5nm dots, spaced 5nm apart.

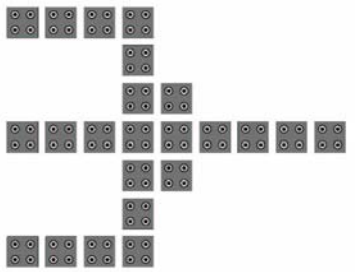

Figure 4. Modified majority gate for $d = d_1$ and d_{NN}.

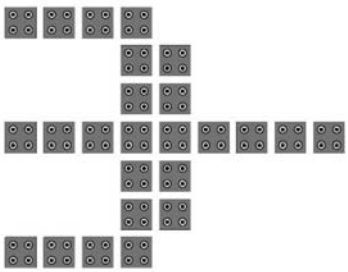

Figure 5. Modified majority gate for d_1, $d = d_{NN}$ and d_2.

zones. However, we will not be able to have clocking zones that are on such a small scale in a desirable design.

The radius of effect-induced faults have now been identified and characterized through simulation. In the next section the new left-to-right majority gates that are tolerant to such radius of effect-induced faults will be proposed.

4: Radius of Effect-Induced Fault-Tolerant Majority Gates

The projected width of a QCA cell for room temperature operation is somewhere in the 5 nm realm. For cells of this size it is not likely that we will be able to have small enough clocking zones (three-cell width in our adder, which will be approximately 75 nm to have working majority gates. Also, in previously proposed adders the clocking zones are non-uniform in that they do not follow the constraints of the proposed clocking scheme. They do not have uniform, parallel, vertical clocking zones that are required by the use of wires running under the array. They are also very inflexible in that, if clocking zones are offset by one or more cells, the array will not properly function. These problems can be solved by creating a majority gate that will operate in a single clocking zone regardless of the radius of effect of the cells.

Therefore, we now have motivation to construct a majority gate that will operate correctly under a single clock control within multiple radius of effect distances. The construction is not complex, in fact it merely involves adding (or subtracting) a number of cells to the gate in order to even out the three inputs' interactions with the device cell(s). First discussed will be the majority gate that will be used to handle a radius of effect of up to d_{NN}.

The modified majority gate can be seen in Figure 4, which is a left-to-right majority gate as is wanted in an adder. From the simulation results in Figure 9, it can be seen that the output for a radius of effect of d_{NN} is correct, and also works for d_1, both with a single clock. This tolerance is facilitated by the addition of only two cells. However, this configuration does not operate correctly with a radius of effect of d_2.

For radius of effect of d_2 we need to add more cells to the configuration. The modified majority gate can be seen in Figure 5. Once again, the addition of one cell to the design creates a structure that will operate correctly with radii of effect d_{NN} and d_2. The simulation results for this configuration are exactly like those seen in Figure 9. Though this modified majority gate cannot handle radius of effect distances of d_3, majority gates that can accept greater distances can be further engineered.

Figure 6 shows a functional clocked majority gate with left inputs and right outputs. The figure

Proceedings of the 2005 20th IEEE International Symposium on Defect and Fault Tolerance in VLSI Systems (DFT'05)
0-7695-2464-8/05 $20.00 © 2005 IEEE

shows that the basic five-cell majority gate is under a different clock cycle than the inputs and outputs. This configuration requires three clocking zones to function properly with a radius of effect of d_{NN}.

Creating QCA structures that will operate at room temperature will require reducing the scale of cells to the molecular level, giving cell sizes of around 2 nm [28]. Molecular cells are constructed by connecting redox sites, which can hold a charge, by ligands that allow tunneling between the sites. A simple example of such a molecule is shown in [29] (1,4-diallyl butane radical cation) and has two allyl groups which are connected by a butyl bridge which facilitates the tunneling of electrons and, therefore, the switching of the molecule between basis states. The size of this molecule is 7 Å in length (0.7 nm). Placing two of these molecules side by side creates a cell with a total of four allyl groups. These four allyl groups act as the dots which contain charges. The two-molecule cell is approximately 1 nm by 1 nm and has the two basic states ("0" and "1") that we need for a typical QCA cell. Cells of this size also have erroneous output in simulation when configured into a left-to-right majority gate.

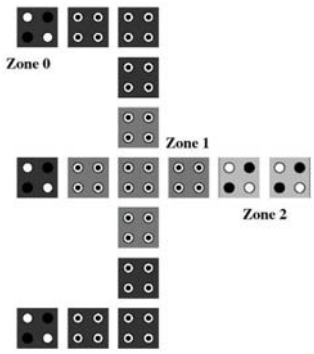

Figure 6. A clocked left-input right-output majority gate using 3 clocking zones. Zones are denoted by shading.

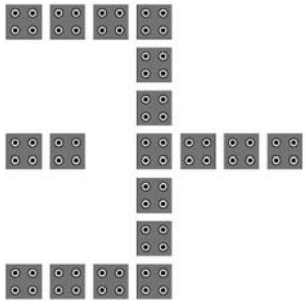

Figure 7. Functioning left-to-right majority gate for cells of size 1, 2, or 4nm.

Cells of width 1 nm, 2 nm and 4 nm were tested in left-to-right majority gates. The results for these configurations were the same for all three-cell sizes and radii of effect d_1 to d_3. All tests resulted in an output equal to the middle input cell. This indicates that the middle input cell overpowers the other inputs at the device cell, switching the device cell to the middle input value at all times. This is not unlike the errors that occur in configurations with larger cells. To overcome this erroneous functioning we have constructed a majority gate that uses one less cell that functions correctly for all three cell sizes and for radius of effect greater than or equal to d_{NN}. The configuration is shown in Figure 7.

For these simulations we used the coherence-vector simulation as with testing of larger cells. The simulations show that this configuration works only for radius of effect greater than or equal to d_{NN}. This fact is obvious since the middle input will only be able to interact with the device cell if it can interact with cells that are d_{NN} away, due to the missing cell in the middle input wire. Through simulation, we have found that this configuration will work for all radii of effect of concern, and beyond.

More accurate simulations were done for molecular implementations of QCA. The coherence vector simulation was used to simulate the previously discussed molecular construction using 1,4-diallyl butane. It is stated in [16] that molecular implementations will have a kink energy (E_k) greater than 500 meV. With this in mind a kink energy of $E_k = 629.45$ (relative permittivity of 0.3) was chosen as an approximate value for the molecule in question. The value was calculated using Equation 10. The simulations were performed at approximate room temperature (300 K). The cell height and width was 1 nm with dot diameter and uniform cell spacing of 0.25 nm.

Proceedings of the 2005 20th IEEE International Symposium on Defect and Fault Tolerance in VLSI Systems (DFT'05)
0-7695-2464-8/05 $20.00 © 2005 IEEE

The simulations show that, under one clock zone, the construction shown in Figure 3 is erroneous, resulting in output equal to the middle input for radius of effect greater than d_{NN}. When the majority gate shown in Figure 7 is used under the same constraints, it functions for radii of effect from d_{NN} to d_3 and beyond. The results of the simulation can be seen in Figure 11. This shows that the radius of effect-induced fault-tolerant majority gate can operate at room temperature for molecular implementations of QCA.

5: Conclusion

It has been shown that radius of effect faults occur in the simplest of structures in quantum-dot cellular automata. Under one clock cycle majority gates will provide erroneous results and, therefore, will limit the clocking scheme when placed in larger arrays.

To counter these faults we have made minor adjustments to the majority gate. It has been shown that these changes, which are made according to the radius of effect of each individual cell, result in functioning majority gates. It has also been shown that, under simulation, the radius of effect-induced fault-tolerant majority gates will operate for molecular implementations of QCA, which is important due to the fact that a molecular level cell will be needed to create arrays that will function at room temperature. It is hoped that these modified majority gates will facilitate more flexible large QCA arrays with respect to clocking.

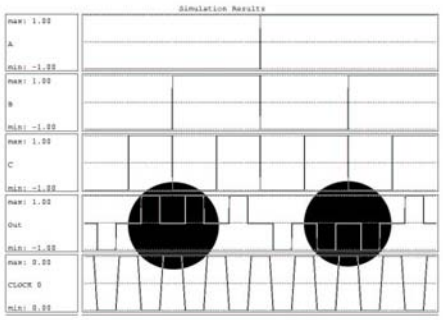

Figure 8. Simulation results for majority gate in figure 3.

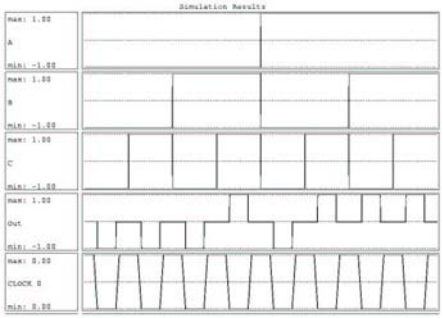

Figure 9. Simulation results for the modified majority gates in figure 4 and figure 5.

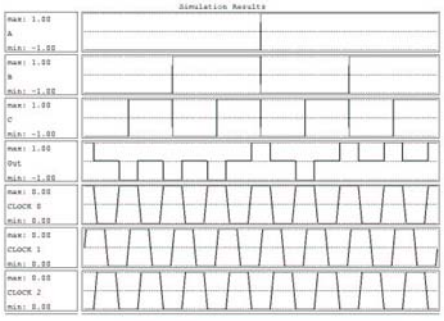

Figure 10. Simulation results for majority gate in figure 6 w ith three clocking zones.

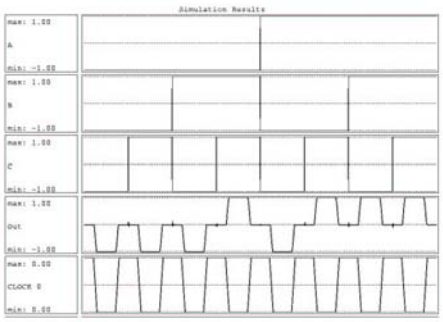

Figure 11. Simulation results for molecular QCA fault-tolerant majority gate.

Proceedings of the 2005 20th IEEE International Symposium on Defect and Fault Tolerance in VLSI Systems (DFT'05)
0-7695-2464-8/05 $20.00 © 2005 IEEE

References

[1] Industry Technology Roadmap for Semiconductors, "Industry Technology Roadmap for Semiconductors (ITRS) 2004," *http://public.itrs.net*, 2004.

[2] G. Snider , A. Orlov, I. Amlani, G. Bernstein, C. Lent, J. Merz and W. Porod, "Quantum-Dot Cellular Automata," Microelectronic Engineering, Vol 47, pp 261-263, 1999.

[3] G. Snider , A. Orlov, I. Amlani, X. Zuo, G. Bernstein, C. Lent, J. Merz and W. Porod, "Quantum-Dot Cellular Automata," Journal of Vacuum Science & Technology A-Vacuum Surfaces and Films, Vol 17, pp 1394-1398, 1999.

[4] G. Toth and C. Lent, "Quasiadiabatic Switching for Metal-Island Quantum-Dot Cellular Automata," Journal of Applied Physics, Vol 85, pp 2977-2984, 1999.

[5] W. Porod, "Quantum-Dot Devices and Quantum-Dot Cellular Automata," International Journal of Bifurcation and Chaos, Vol 7, pp 2199-2218, 1997.

[6] W. Porod, "Quantum-Dot Devices and Quantum-Dot Cellular Automata," Journal of the Franklin Institute-Engineering and Applied Mathematics, Vol 334B, pp 1147-1175, 1997.

[7] P. Tougaw and C. Lent, "Quantum Cellular-Automata - Computing with Quantum-Dot Molecules," Compound Semiconductors, Vol 141, pp 781-786, 1995.

[8] C. Lent, P. Tougaw, W. Porod and G. Bernstein, "Quantum Cellular Automata," Nanotechnology, Vol 4, pp 49-57, 1993.

[9] F. Rojas, E. Cota and S. Ulloa, "Magnetic Field and Dissipation Effects on the Charge Polarization in Quantum Cellular Automata," IEEE Transactions on Nanotechnology, Vol 3, pp. 41-, 2004.

[10] R. Kummamuru, J. Timler, G. Toth, C. Lent, R. Ramasubramaniam, A. Orlov, G. Bernstein and G. Snider, "Power Gain in a Quantum-Dot Cellular Automata Latch," Applied Physics Letters, Vol 81, pp 1332-1334, 2002.

[11] M.B. Tahoori, M. Momenzadeh, J. Huang and F. Lombardi, "Defects and Faults in Quantum Cellular Automata," VLSI Test Symposium, 2004.

[12] "QCADesigner: The QCA simulator homepage," *http://www.atips.ca/projects/qcadesigner*, 2004.

[13] "QCADesigner," *http://www.qcadesigner.ca*, 2004.

[14] J. Timler and C. Lent, "Power gain and dissipation in quantum-dot cellular automata," J. Appl. Phys., Vol 91, pp 823-831 2002.

[15] G. Toth and C. Lent, "Quantum computing with quantum-dot cellular automata," A Physical Review, Vol 63, 2001.

[16] J. Timler and C. Lent, "Maxwell's demon and quantum-dot cellular automata," J. Appl. Phys., Vol 94, pp 1050-1060, 2003.

[17] A. I. Csurgay and W. Porod and C. S. Lent, "Signal Processing with Near-Neighbor-Coupled Time-Varying Quantum-Dot Arrays," IEEE Trans. Circuits Syst. I, Vol 47(8), pp 1212-1223, 2000.

[18] M. T. Niemier, A. F. Rodrigues and P. M. Kogge, "A Potentially Implementable FPGA for Quantum Dot Cellular Automata," Proc. NSC, Vol 1, 2002.

[19] A. Vetteth, K. Walus, V. S. Dimitrov and G. A. Jullien, "Quantum-dot Cellular Automata Carry-Look-Ahead Adder and Barrel Shifter," Proc. IEEE ETTC, 2002.

[20] C. D. Armstrong and W. M. Humphreys, "The Development of Design Tools for Fault Tolerant Quantum Dot Cellular Automata Based Logic," 2nd International Workshop on Quantum Dots for Quantum Computing and Classical Size Effect Circuits, 2003.

[21] C. D. Armstrong, W. M. Humphreys and A. Fijany, "The Design of Fault Tolerant Quantum Dot Cellular Automata Based Logic, 11th NASA Symposium on VLSI Design, 2003.

Proceedings of the 2005 20th IEEE International Symposium on Defect and Fault Tolerance in VLSI Systems (DFT'05)
0-7695-2464-8/05 $20.00 © 2005 IEEE

[22] M. Governale, M. Macucci, G. Iannaccone and C. Ungarelli, "Modeling and manufacturability assessment of bistable quantum-dot cells," J. Appl. Phys., Vol 85, pp 2962-2971, 1999.

[23] C. G. Smith, "Computation Without Current," Science, Vol 284, pp 5412, 1999.

[24] A. O. Orlov and I. Amlani, "Realization of a Functional Cell for Quantum-dot Cellular Automata," Science, Vol 277, pp 5328, 1997.

[25] P. D. Tougaw and C. S. Lent, "Dynamic behavior of quantum cellular automata," J. Appl. Phys., Vol 80, pp 4722-4736, 1996.

[26] I. Amlani, A. O. Orlov, G. L. Snider and C. S. Lent, "Demonstration of a six-dot quantum cellular automata system," Appl. Phys. Letters, Vol 72, pp 2179-2181, 1998.

[27] S. E. Frost, A. F. Rodrigues, A. W. Janiszewski, R. T. Rausch and P. M. Kogge, "Memory in Motion: A Study of Storage Structures in QCA," Proc. NSC, Vol 1, 2002.

[28] M. Lieberman, S. Chellamma, B. Varughese, Y. Wang, C. Lent, G. H. Bernstein, G. Snider, and F. C. Peiris, "Quantum-Dot Cellular Automata at a Molecular Scale," Ann. N.Y. Acad. Sci, Vol 960, pp 225-239, 2002.

[29] C. Lent, B. Isaksen, and M. Lieberman, "Molecular Quantum-Dot Cellular Automata," J. Am. Chem. Soc., Vol 125, pp 1056-1063, 2003.

Proceedings of the 2005 20th IEEE International Symposium on Defect and Fault Tolerance in VLSI Systems (DFT'05)
0-7695-2464-8/05 $20.00 © 2005 IEEE